THE PROPERTIES OF PLASMA FLOWS IN FINE RAY STRUCTURES OF THE STREAMER BELT

V. G. ESELEVICH and M. V. ESELEVICH
Institute of Solar-Terrestrial Physics, Irkutsk, Russia (E-mail: esel@iszf.irk.ru)

(Received 27 September 1999; accepted 14 July 2000)

Abstract. We show that within distances from the Sun's surface less than the height of a streamer helmet, each of two neighboring rays of the streamer belt, as they approach the solar surface, bends around the helmet on either side of it. Also, a minimum angular diameter of the rays of $d \approx 2^\circ$–3° remains virtually constant within $R = 1.2$–$6.0\ R_\odot$. A density inhomogeneity ('blob') can be produced above the helmet top visible to at least $R \approx 6\ R_\odot$. In this case the initial velocity of the 'blob' increases with solar distance from where it is generated to something like the velocity of the bulk solar wind with which the 'blob' is carried away.

1. Introduction

In our most recent paper (Eselevich and Eselevich, 1999, hereinafter Paper 1) based on the LASCO C2 and C3 data, we have shown that within distances $R > 3$–$4\ R_\odot$ from the Sun's center the streamer belt, in the absence of coronal mass ejections (CMEs), constitutes a sequence of radial rays of increased brightness. A minimum angular diameter of an individual ray $d \approx 2^\circ$–3°, and its lifetime may be as long as 10 days. Outward motions of mass inhomogeneities with a typical time scale of about several hours are produced in a random fashion within the rays. Plots of their velocity increase with increasing R are similar to those obtained by Sheeley *et al.* (1997) for a 'blob' carried by the bulk solar wind. Hence there is evidently a strong case for the fact that in the absence of CMEs, in the streamer belt there appear to exist both the bulk solar wind, whose characteristics vary relatively slowly with time, and sporadic wind flows with a characteristic lifetime of about a few hours or shorter. The latter type should also include the recently discovered, both sunward and anti-sunward directed, sporadic plasma streams arising due to the decay of a streamer, presumably as a result of the reconnection process of magnetic field lines (Wang *et al.*, 1999a, b).

These results raise several questions for researchers with regard to the formation origin of the various types of plasma flows in the streamer belt, of which the most important, top priority problems were formulated by Wang *et al.* (1998).

The objective of this paper is to investigate fine ray structures of the streamer belt within $1.2\ R_\odot < R < 6\ R_\odot$, and plasma flow properties inside the rays. Specifically: places of initiation and some characteristics of 'blobs'; the existence

Solar Physics **197:** 101–113, 2000.

and velocity of the bulk solar wind within which 'blobs' are embedded; and the place of initiation of the bulk solar wind.

2. Data and Methods of Analysis

2.1. THE DATA ANALYZED

White-light corona brightness data from the LASCO C1 and C2 instruments on the SOHO spacecraft were used in the investigations reported here. The C1 coronagraph provides white-light corona images for 1.1–3.0 $R_\odot$ while C2 coverage is 2–6 $R_\odot$. Daily images in the MPEG format were used. The interframe time did not exceed, on the average, one hour. Selected data for 1996 and 1998 were used in the analysis. To minimize the possible influence of the features of the data analyzed we have adhered to the following principles:

(1) Only bright enough ray structures (whose brightness markedly exceeded the surrounding background) within $R = 1.2$–6.0 $R_\odot$ from the Sun's center were investigated.
(2) Emphasis in our study was placed not on absolute brightness distributions of the corona but on their relative variations with time. Also, the time interval in each case under investigation did not exceed several days. This permitted us to eliminate the influence of possible gradual changes in instrument performance over the course of time.
(3) We studied radial structures in the corona, with the projection Λ of their latitude onto the plane of the sky not exceeding $\pm 50°$. Λ is positive northward of the equator and negative southward.

2.2. DETERMINING THE RAY BRIGHTNESS, P_R, AND THE ANGULAR SIZE OF RAYS, d, IN THE STREAMER BELT

For each image obtained from daily MPEG files, we constructed brightness distributions P of the corona depending on the angle Λ at different distances R from the Sun's center, separately for the E and W limbs. To investigate the ray properties we introduce the following characteristics (Paper 1): the ray brightness P_R and the angular size of the ray d. The ray is distinguished in the brightness profile P by the slope of two lines forming it, which from the top P_M, maximum brightness of the ray, to the inflection points A and B, may be represented by straight lines. This permits us to introduce the determination of the ray brightness P_R and angular size d, as shown in the upper panels of Figures 1 and 2 from Paper 1. Also, the angular size of the ray in any direction is assumed to be the same. To unify the process of identifying the ray on the background of the remainder of the signal and, accordingly, determining the ray brightness P_R and angular size d, we proceeded as follows: for each profile P, we produced a smooth curve P_S by averaging over an angle of 6–7 deg. After that, the averaged curve was subtracted from the original

profile P to give the curve $\Pi = P - P_S$, based on which the brightnesses of individual rays were determined from the relation $P_R = P_M - P_S$.

3. The Ray Structure of the Streamer Belt within $R = 1.2–6.0\ R_\odot$

3.1. THE STREAMER BELT PERPENDICULAR TO THE PLANE OF THE SKY

In Paper 1 we have shown that within $R > 3–4\ R_\odot$, i.e., above the helmet top of the streamer, brightness rays that constitute the streamer belt are oriented virtually radially and their minimum angular size is close to $d \approx 2.0–3.0°$. Our prime interest here is the configuration of these rays below the helmet top, i.e., at $R < 3–4\ R_\odot$. Let us consider the typical event of July 21, 1996 (12:58 UT) (W-limb) when a sufficiently extended ($\approx 50–100°$) portion of the plane of the streamer belt was almost perpendicular to the plane of the sky. In this case the limb exhibits a single narrow, radial ray with $d \approx 2.0–3.0°$, with the streamer helmet lying at its base at $R < 3–4\ R_\odot$. Consider the behavior of the ray structures below the helmet top of the streamer and how they are associated with the radial ray at $R > 3–4\ R_\odot$. Figure 1 shows the distributions $\Pi = P - P_S$ of the corona depending on the angle Λ for two distances R below the helmet top, Figure 1 (upper panel, $R = 2.4\ R_\odot$, and middle panel, $R = 3.0\ R_\odot$), and for one distance above the helmet, Figure 1 (lower panel, $R = 5.0\ R_\odot$) for the W limb.

It is evident from Figure 1 that two rays bend around the helmet profile; with increasing distance from the Sun, these rays come gradually closer together to merge into a single ray above the helmet top. This picture is clearly seen in Figure 2, in which we constructed (based on using a set of $P(\Lambda)$-profiles for different R) in the plane $R/R_\odot - \Lambda$ the position curves for the following typical points of the rays: the tops A and B (solid lines), the points D and G at the heights respectively $\Pi(D) = \Pi(A) - 2P_R(A)/3$, and $\Pi(G) = \Pi(B) - 2P_R(B)/3$, and the points E and F at the heights, respectively $\Pi(E) = \Pi(A) - 2[\Pi(A) - \Pi(C)]/3$, and $\Pi(F) = \Pi(B) - [\Pi(B) - \Pi(C)]/3$ and a minimum between rays of the point C.

Generally, the ray bifurcation below the helmet top can result from features of the background, which is subtracted from images of the MPEG files. To exclude the influence of this factor, the distributions $\Pi = P - P_S$ were constructed depending on the angle Λ at distances R below and above the helmet top for: a) the FITS file ($\approx$ 274 kb) with the C2 image on 21 July 1996 (04:20 UT), containing comprehensive information without the subtracted background; and b) the polarization brightness with the C2 image on 21 July 1996 (19:42 UT) (these data were kindly made available to us by Dr Yi-Ming Wang).

In both cases it was shown that the helmet profile was skirted by two rays which, with distance from the Sun, come gradually closer together, and above the helmet top they merge into one ray.

It is suggestive from Figure 2 that a neutral line passes near the helmet top (asterisk), which separates the magnetic field line arch delineating the streamer helmet

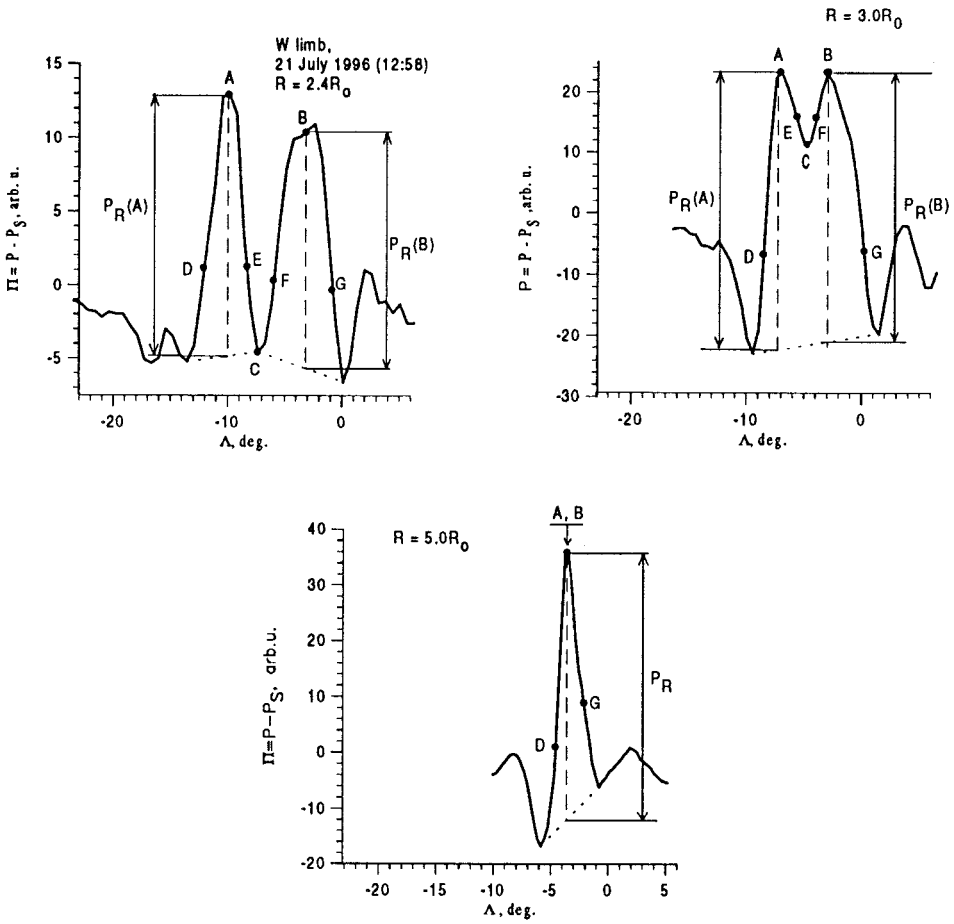

Figure 1. Ray brightness distribution Π profiles versus angle Λ for the portion of the streamer belt perpendicular to the plane of the sky, at three different distances from the Sun's center: below the helmet top (*upper left panel*) $R = 2.4\ R_\odot$, and (*upper right*) $R = 3.0\ R_\odot$; above the helmet top (*lower panel*) $R = 5.0\ R_\odot$. Data from LASCO C2 for 21 July 1996, 15:58 UT, W limb.

into two parts with opposite directions of the radial magnetic field. Two rays of increased brightness skirting the helmet on both of its sides are directly adjacent to the portions of this arch. Therefore, each of them can have the same direction of the magnetic field as the adjacent portion of the arch. This means that the direction of the magnetic field in the right and left rays can be opposite (shown by the arrows). Since the rays are magnetic flux tubes with high-conductivity plasma, they cannot penetrate each other. We must therefore assume that above the helmet top the rays (magnetic tubes) extend along a line following each other. This is consistent with the view that the streamer belt consists of a sequence of rays with a typical angular size of several degrees (Paper 1).

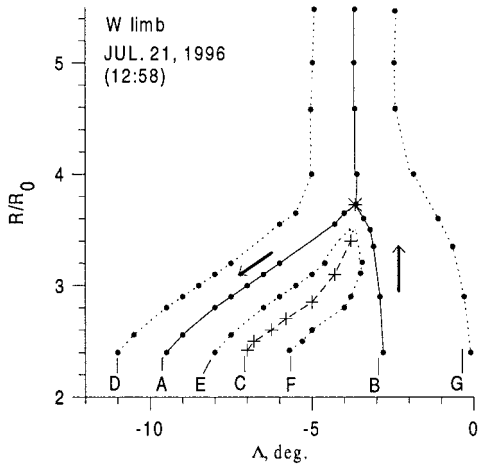

Figure 2. Position curves in the plane $R/R_\odot - \Lambda$ for the following characteristic points of ray brightness shown in Figure 1: tops of rays A and B (*solid lines*), points D and G at the heights respectively $\Pi(D) = \Pi(A) - 2P_R(A)/3$ and $\Pi(G) = \Pi(B) - 2P_R(B)/3$, and the points E and F at the heights, respectively $\Pi(E) = \Pi(A) - 2[\Pi(A) - \Pi(C)]/3$ and $\Pi(F) = \Pi(B) - [\Pi(B) - \Pi(C)]/3$, and a minimum between rays of the point C. The neutral line is indicated by an asterisk. The arrows indicate the magnetic field direction in the rays.

If it is assumed that the direction of the magnetic field in brightness tubes skirting the streamer helmet is opposite (which requires extra evidence), then Figure 2 suggests a new, quite surprising result: in each pair of adjacent tubes in the streamer belt the direction of the magnetic field is opposite! Several events similar to the event under consideration were detected and investigated. Nevertheless, we feel that it is opportune to call the reader's attention to this result, because if it is confirmed, this would produce important implications for the physical modeling of streamers. It should also be noted that it is perhaps this specific character (opposite signs of field in adjacent rays (magnetic tubes)) which is responsible for the fact that the ray structure of streamers becomes unstable to the formation process of 'blobs' which occur rather frequently.

3.2. THE STREAMER BELT NEARLY IN THE PLANE OF THE SKY

Let us consider the W-limb event of 2 January 1998 (13:32–13:39 UT) when a portion of the neutral line extended along the meridian near longitudes 350–360° on the CR 1931 synoptic map intersecting the W-limb plane of the sky (according to J. T. Hoeksema's data), i.e., the portion of the streamer belt under consideration lay nearly in the plane of the sky. Figure 3 shows the corona's brightness distributions P depending on the angle Λ at R =1.27 $R_\odot$ – below the helmet top (left panel in Figure 3) and $R = 4.5\ R_\odot$ – above the helmet (right panel in Figure 3) for the W limb.

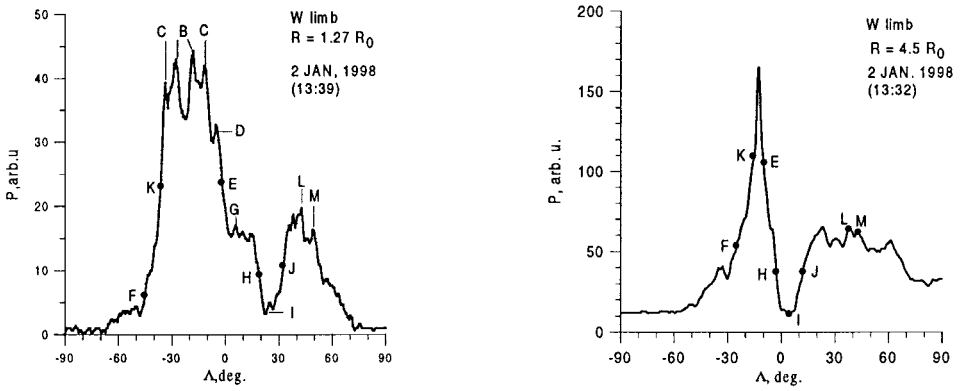

Figure 3. Brightness distribution P profiles versus angle Λ for the portion of the streamer belt lying nearly in the plane of the sky, for two different distances from the Sun's center below the helmet top (*left panel*) $R = 1.27\ R_\odot$; above the helmet top (*right panel*) $R = 4.5\ R_\odot$. Data from LASCO C1 and C2, January 02, 1998 (respectively, 13:39 and 13:32 UT), W limb.

In both figures, the letters designate characteristic portions of the profile $P(\Lambda)$, most of which may be sufficiently reliably traced out from within 1.2 $R_\odot$ to about 1.8 $R_\odot$ according to the C1 data and from 2.3 $R_\odot$ to 6 $R_\odot$ according to the C2 data. Here the letters B, C label the loops; D, G, K, L correspond to rays; F, K, E, H, J refer to the position of the midpoints of the most pronounced jumps of brightness; and I labels the position of a brightness minimum. The characteristic points of brightness gradients, F, K, E, H, J (Figure 4) are traceable best of all.

Rays D and G are impossible to trace out beyond 2.0–2.5 $R_\odot$. Figures 3 and 4 suggest that the brightness gradients labeled by the points K and E are the outer boundaries of two rays (or magnetic tubes), possibly with an opposite direction of the magnetic field (shown by the arrows in Figure 4). As in the case of the event in Figure 2, at distances $R >$3–4 $R_\odot$ (above the helmet top) these rays merge into a single, radially oriented ray with an angular width of $\approx 2.5°$. Of the rays lying in the belt's plane, rays L and M are traceable out to large enough distances. In this case, within $R = 1.27\ R_\odot$ to $R = 4.3\ R_\odot$, rays L and M depart from a radial direction by about 4° and 6°, respectively (Figure 4). At $R > 4\ R_\odot$, both rays are virtually radial. As is evident from Figure 5, the angular size of these rays is $\approx 3.6°$ (ray L) and $\approx 2.7°$ (ray M) and remain almost unchanged with distance from the Sun, at $R = 1.2$–$6.0\ R_\odot$. It is intriguing that the angular size of closed solar loops B, C is also close to the value ≈ 2–$4°$.

4. Motion of Inhomogeneities in Ray Structures

In Paper 1, the dependencies of the leading edge velocity of inhomogeneities on the distance R from the Sun, $V(R)$, were investigated both for a maximum of total ray brightness P_M and for the ray brightness P_R (see Figures 5 and 6 and the

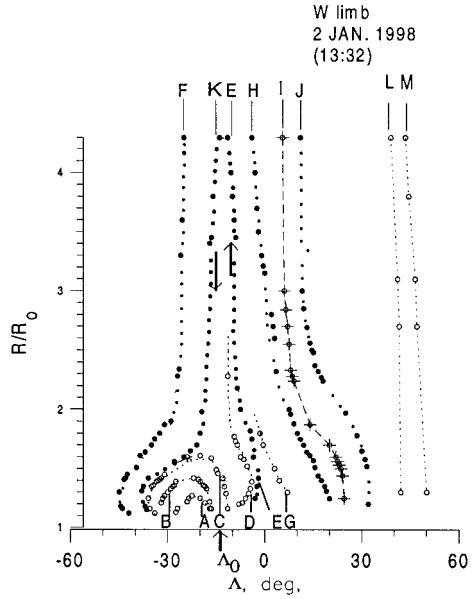

Figure 4. Position curves on the plane $R/R_\odot - \Lambda$ for the following characteristic points of the distributions $P(\Lambda)$ shown in Figure 3: A, B, C – brightness maxima corresponding to loops; D, G, K, L – brightness maxima corresponding to rays; F, K, E, H, J – positions of the midpoints of the most conspicuous jumps of brightness, I – positions of a brightness minimum.

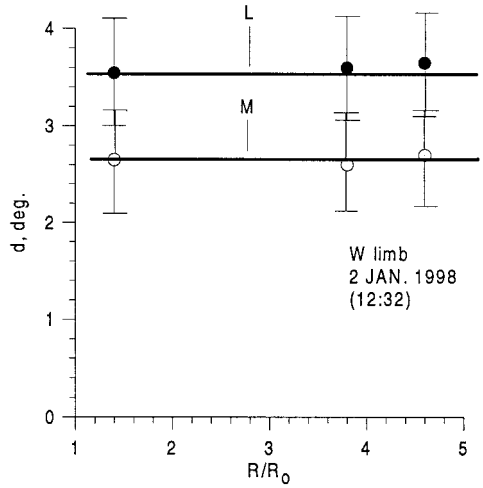

Figure 5. The angular sizes of rays L and M shown in Figure 4, depending on the distance $R/R_\odot$.

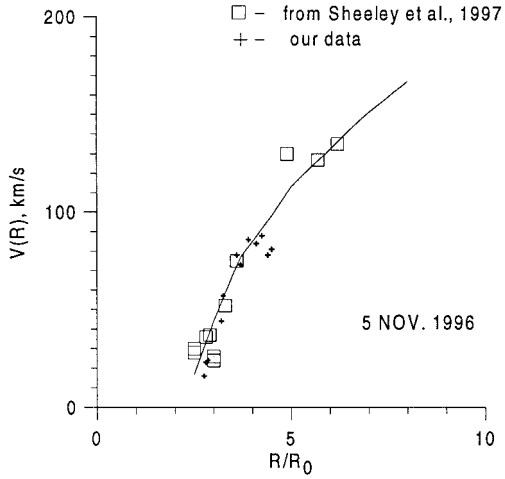

Figure 6. Dependence of the 'blob's' velocity on $R/R_\odot$: *boxes* – from a paper of Sheeley *et al.* (1997), *crosses* – our result. Data from LASCO C2, 5 November 1996, W limb, $\Lambda \approx -1.5°$.

appropriate text in Paper 1). Both methods of plotting yield approximately the same $V(R)$-dependencies. (The possible difference between the terms plasma inhomogeneity and 'blob' will be explained later in the text.) The method of measuring the velocity V was as follows: arrival times of the brightness inhomogeneity front were determined for the ray selected (i.e., the position of a brightness maximum P_M or a ray brightness P_R of this ray) for different distances R. After that, the known length of the path and the travel time were used to determine the mean velocity V of the front along this length. Figure 6 for the event of 5 November 1996 shows the $V(R)$-dependence obtained by this method (crosses) and by the method from Sheeley *et al.* (1997) (boxes). One can see a good agreement between results from both methods.

In order to minimize the vignetting influence and other possible effects within the LASCO C2 instrument on the measuring accuracy of the leading edge velocity we proceeded as follows: the portions ΔR between two neighboring distances R_i and R_{i+1}, at which the mean velocity of the inhomogeneity leading edge was determined, were taken as small as possible. For instance, at $R \leq 4\ R_\odot$ the value of $\Delta R \approx 0.1{-}0.3\ R_\odot$ with the typical front width $\delta R \approx 0.5\ R_\odot$. The advantage of our method is that it permits us to study the dynamics of the inhomogeneity profile in space and in time, as well as to investigate in more detail the $V(R)$-dependencies in its initial portion at small velocities. One finding of such an investigation is illustrated in Figure 7 for the event of 29–30 June 1996.

The figure clearly shows two portions of the $V(R)$-dependence: a slow (at $R < 4\ R_\odot$) and faster ($R > 4\ R_\odot$) velocity increase with distance R. This dependence may be logically interpreted as follows. The portion of a slow velocity increase at $R < 4\ R_\odot$ corresponds to the movement of the density inhomogeneity with the bulk solar wind speed which carries it away. When the inhomogeneity

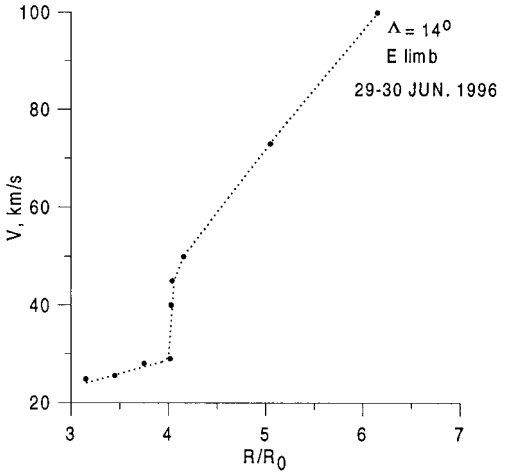

Figure 7. Velocity dependence of the plasma density inhomogeneity front on $R/R_\odot$. Transition of the inhomogeneity to the state of a 'blob' at $R \approx 4.0\ R_\odot$. Data from LASCO C2, 29–30 July 1996, E limb, $\Lambda \approx 14°$.

front reaches the distance $R \approx 4\ R_\odot$, some unknown process (conceivably 'reconnection') induces a local rearrangement of the magnetic field and, perhaps, a fast plasma heating. As a result, the inhomogeneity is turned to a 'blob', with an abrupt increase of its velocity. This brings up the question: is the place of origin of the leading edge of the 'blob' (i.e., of its part at the greatest distance from the Sun) associated with the top of the streamer helmet? To answer this question, we turn to the event of 1–2 January 1998. Figure 8 shows the $P_M(t)$-dependencies at different distances R for the selected brightness ray when $\Lambda \approx -14°$ (indicated on the axis Λ_0 in Figure 4) on the west limb.

Crosses show the middles of the fronts of individual inhomogeneities. It is evident from Figure 8 that front 1 starts moving (time displacement of the cross to the right with respect to the vertical dashed line with increasing R) at $R < 3.8\ R_\odot$ (or, more exactly, at $R \approx 3.4\ R_\odot$), front II at $R \geq 4.2\ R_\odot$, front III at $R \geq 4.2\ R_\odot$, and front IV at $R \geq 4.6\ R_\odot$. Let the distance beyond which the front is observed to move, be designated as $R = R_m$. It follows from Figure 8 that front IV, representing a small jump of brightness $\Delta P \approx 5$ arb.u., exists and is fixed within $3.8\ R_\odot < R < R_m$; it is absent at $R \leq 3.8\ R_\odot$. This means that within 3.8 $-4.6\ R_\odot$, i.e., along the length $\Delta \approx 0.8\ R_\odot$, there is a rapid temporal increase in brightness by the amount of the jump ΔP observed as front IV. Upon leaving this portion toward $R > 4.6\ R_\odot$, one immediately finds this front to move. A similar situation occurs for the other fronts, although the corresponding portions of brightness increase have somewhat different lengths Δ (but comparable with $R_\odot$), and the start of their motion occurs at different R_m. Velocity dependencies on R for fronts I, III and IV are plotted in Figure 9.

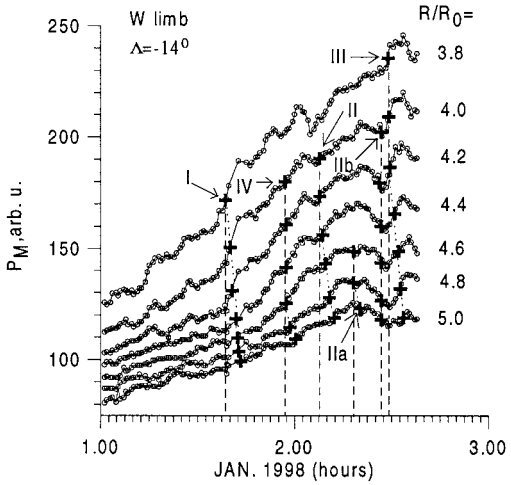

Figure 8. Time dependencies of a brightness maximum P_M for the ray representing a cross-section of the streamer belt normal to the plane of the sky on W limb for different distances $R/R_\odot$. 1–2 January 1998, W limb, $\Lambda \approx -14°$.

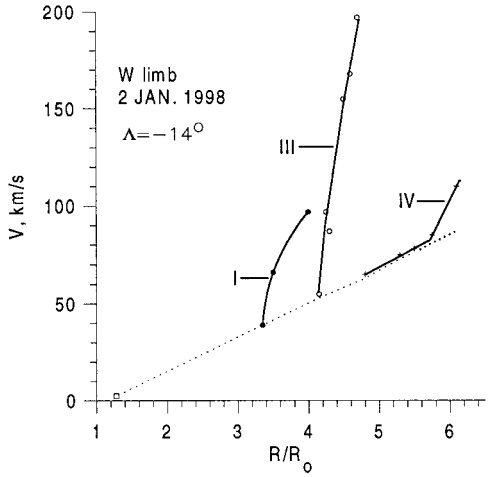

Figure 9. Velocity dependencies of the fronts of several plasma density inhomogeneities on $R/R_\odot$. *Dashes* – speed of the main solar wind which carries the inhomogeneity. Data from LASCO C2, 2 January 1998, W limb, $\Lambda \approx -14°$ (*dark and open circles*, *crosses*), $\Lambda \approx 4°$ (*box*).

The box at $R = 1.3\ R_\odot$ indicates the velocity of the front of a plasma density inhomogeneity (according to the C1 data) as measured inside ray $E(\Lambda = 4)$ in Figure 4. (Velocity measurements of the inhomogeneity front from the C1 data have a large error (of order 100%) and are only possible for some of the portions of the ray selected). Dashes in Figure 9 interconnect the values of minimum velocities V_w recorded for inhomogeneities (or 'blobs') appearing at different R. As can be seen, the values of V_w increase with the distance from the Sun. Inhomogeneity front IV

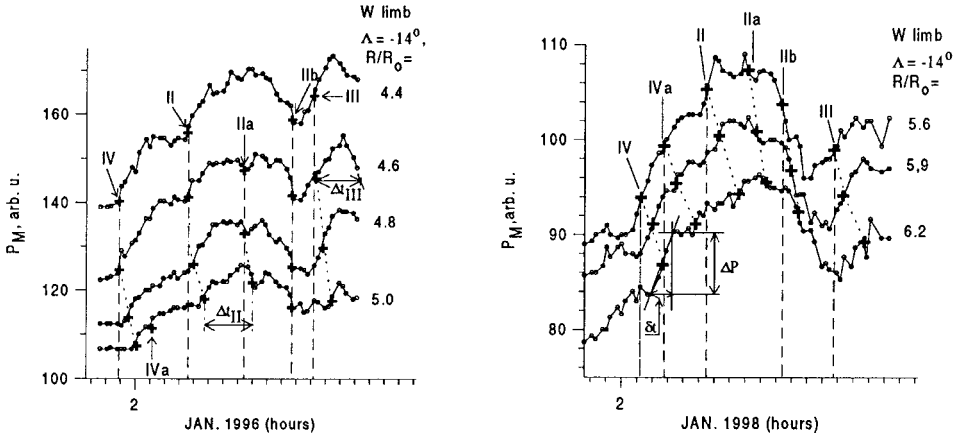

Figure 10. The selected portion of the dependencies of a brightness maximum P_M from Figure 8, for different $R/R_\odot$, on an enlarged scale.

has two portions: a gentle one, lying along the dashed curve, and a steeper portion. The dashed curve in Figure 9 may be interpreted as the $V_w(R/R_\odot)$-dependence for the bulk solar wind which carries inhomogeneities (or 'blobs'). The $V(R/R_\odot)$-dependence for front IV in Figure 9 is similar to the event in Figure 7 considered above. To estimate the typical size of density inhomogeneities and their dynamics with distance R, we now turn our attention to Figure 10 (left and right panels) where the portion of the $P(t)$-dependencies, including fronts II, III, and IV, is drawn on an enlarged scale.

First of all, we wish to point out some characteristic properties revealed by visual examination of these figures. Front II is seen to be followed by two fronts with a temporally decreasing 'inverse' density gradient, IIa and IIb, which travel with about the bulk solar wind speed V_w (dashes in Figure 9). An 'inverse' front of small amplitude IIa exists and is fixed within $R = 4$–$5\ R_\odot$ (i.e., along the length $l \approx R_\odot$) and starts to move with a velocity close to V_w at $R > 5\ R_\odot$. The width of front IV at $R = 4.8\ R_\odot$ is estimated at $\delta \approx \delta t V \approx 0.3\ R_\odot$. Here δt is the time width of the front, and V is its velocity. At $R = 6.2\ R_\odot$, δ reaches the value $0.6\ R_\odot$. (Determination of δt and ΔP is from lower panel of Figure 10.) Since fronts II and IIa at $R = 4.8$–$5.0\ R_\odot$ travel with about the same velocity V_w it is possible to estimate the inhomogeneity size Δ_{II} with leading edge II and trailing edge IIa (see Figure 10, left and right panels): at $R = 5\ R_\odot$ we have $\Delta_{\mathrm{II}} \approx 0.9\ R_\odot$. The inhomogeneity with the leading edge III at $R = 4.6\ R_\odot$ is estimated as $\Delta_{\mathrm{III}} \approx 1\ R_\odot$. Thus the size Δ of the inhomogeneities under consideration does not exceed 1–$2\ R_\odot$, and they have their origins above the top of the streamer helmet ($R = 2\ R_\odot$ for the event under consideration) for any one of $R < 6.5\ R_\odot$. (In Figure 10 (left panel) the formation of front IVa (most distant from the Sun) occurs at $R = 5.0\ R_\odot$.)

5. Conclusions

(1) At distances R that are smaller than the height of the streamer helmet, each of the two adjacent rays, as they approach the solar surface, passes around the helmet on either side thereof. Also, a minimum angular size of the rays, $\approx 2-3^\circ$, remains virtually constant at $R = 1.2-6.0\ R_\odot$.

(2) A 'blob' can be produced above the helmet top within distances of up to $R \approx 6\ R_\odot$ at least, which is in agreement with results reported by Sheeley *et al.* (1997, Figure 6).

(3) The initial velocity of the 'blob' increases with the solar distance at which it is produced, and is about the speed of the bulk solar wind which carries it away.

Acknowledgements

The SOHO/LASCO data used here are produced by a consortium of the Naval Research Laboratory (USA), Max-Planck-Institute für Aeronomie (Germany), Laboratoire d'Astronomie (France), and the University of Birmingham (U.K.). SOHO is a project of international cooperation between ESA and NASA.

Wilcox Solar Observatory data used in this study were obtained via web site http://quake.stanford.edu/wso at 1998:05:14_ 18:43:35 PDT courtesy of J. T. Hoeksema. The Wilcox Solar Observatory is supported by NASA, NSF, and ONR. We are grateful to V. G. Mikhalkovsky for his assistance in preparing the English version of the manuscript. Grant governmental support for Russian Federation's leading scientific schools N961596733 and GNTP 'Astronomy'.

References

Burlaga, L. F., Hundhausen, A. J., and Zhao, X.: 1981, *J. Geophys. Res.* **86**, 8893.
Crooker, N. U., Siscoe, G. L., Shodhan, S., Webb, D. F., Gosling, J. T., and Smith, E. J.: 1993, *J. Geophys. Res.* **98**, 9371.
Eselevich, V. G.: 1998, *J. Geophys. Res.* **103**, 2021.
Eselevich, V. G. and M. V. Eselevich: 1999, *Solar Phys.* **188**, 299 (Paper I).
Gosling, J. T., Borrini, G., Asbridge, J. R., Bame, S. J., Feldman, W. C., and Hansen, R. T.: 1981, *J. Geophys. Res.* **82**, 5438.
Illing, R. M. E. and Hundhausen, A. J.: 1986, *J. Geophys. Res.* **91**, 951.
Korzhov, N. P.: 1977, *Solar Phys.* **55**, 505.
Sheeley, N. R. Jr. *et al.*: 1997, *Astrophys. J* **484**, 472.
Svalgaard, L., Wilcox, J. M., and Duvall, T. L.: 1974, *Solar Phys.* **37**, 157.
Wilcox, J. M. and Hundhausen A. J.: 1983, *J. Geophys. Res.* **88**, 8095.
Wang Y.-M. *et al.*: 1997, *Astrophys. J.* **485**, 875.
Wang Y.-M. *et al.*: 1998, *Astrophys. J.* **498**, L165.

Wang Y.-M., Sheeley, N. R., Jr., Howard, R. A., St. Cyr, O. C., and Simnett, G. M.: 1999a, *Geophys. Res.* **26**, 1203.
Wang Y.-M., Sheeley, N. R., Jr., Howard, R. A., Rich, N. B., and Lamy, P. L.: 1999b, *Geophys. Res.* **26**, 1349.